

Noninvasive measurement of aminolevulinic acid-induced protoporphyrin IX fluorescence allowing detection of murine glioma *in vivo*

Summer L. Gibbs-Strauss*[†]

Julia A. O'Hara

Dartmouth College
Thayer School of Engineering
Hanover, New Hampshire 03755

P. Jack Hoopes

Dartmouth College
Thayer School of Engineering and
Department of Surgery
Hanover, New Hampshire 03755

Tayyaba Hasan

Harvard Medical School
Massachusetts General Hospital
Wellman Center for Photomedicine
Boston, Massachusetts 02114

Brian W. Pogue*

Dartmouth College
Thayer School of Engineering
Hanover, New Hampshire 03755
and
Wellman Center for Photomedicine
Massachusetts General Hospital
Boston, Massachusetts 02114

1 Introduction

Aminolevulinic acid (ALA), the precursor to protoporphyrin IX (PpIX), has been under extensive study as a photosensitizer for photodynamic therapy (PDT) and for photodiagnosis (PD) in oncology for more than 20 years.¹ While much of the focus with ALA detection of tumors has been in thin squamous tissues, perhaps one of the most successful applications of ALA-PpIX for fluorescence visualization, and certainly the most important to the work presented here, has been the use of ALA-induced PpIX for surgical guidance of brain tumor resection due to demonstration of high PpIX signal in the tumor tissue compared to the normal brain.²⁻⁴ The use of this contrast agent to detect tumors noninvasively has seen little study, yet transmission of the fluorescence through bulk tissue up to several centimeters is readily feasible. With postprocessing of the signal to normalize for attenuation and to provide spectral filtering to remove background, it is feasible to develop noninvasive tools for detection of tumors and tracking the production of PpIX at the tissue surface for a variety of

Abstract. Aminolevulinic acid (ALA)-induced protoporphyrin IX (PpIX) fluorescence is studied as a contrast agent for noninvasive detection of murine glioma, using the fluorescence-to-transmission ratio measured through the cranium. Signals measured prior to administration of ALA are very similar between control animals, 9L-GFP, and U251 tumor-bearing animals. However, 2 h after ALA administration, the PpIX signal from both tumor-bearing groups is significantly higher than the control group (9L-GFP group p -value=0.016, and U251 group p -value=0.004, relative to the control group). The variance in signal from the 9L-GFP group is much larger than either the control group or the U251 group, which is consistent with higher intrinsic PpIX fluorescence heterogeneity as seen *in situ* at *ex vivo* analysis. Decreasing the skin PpIX fluorescence via intentional photobleaching using red light (635 nm) is examined as a tool for increasing PpIX contrast between the tumor-bearing and control groups. The red light bleaching is found to increase the ability to accurately quantify PpIX fluorescence *in vivo*, but decreases the specificity of detection between tumor-bearing and nontumor-bearing groups. © 2009 Society of Photo-Optical Instrumentation Engineers. [DOI: 10.1117/1.3065543]

Keywords: aminolevulinic acid; protoporphyrin IX; glioma; fluorescence; spectroscopy.

Paper 08193RR received Jun. 25, 2008; revised manuscript received Nov. 11, 2008; accepted for publication Nov. 16, 2008; published online Jan. 26, 2009.

orthotopic murine tumors, both implanted and of transgenic origin. This study has focused on these aspects of the problem in the context of murine glioma.

Administration of ALA overloads the heme synthesis pathway, which exists in all mammalian cells, and fluorescently detectable levels of PpIX are produced.⁵⁻⁷ ALA-induced PpIX is now used extensively in dermatologic applications, with approval for treatment of actinic keratosis in the United States in 1999.⁸ Methyl-aminolevulinic acid (MAL), an ester derivative of ALA, has been approved in Europe for treatment of skin lesions.⁸ One confounding factor in detection is the heterogeneity of PpIX production between tumor subtypes and even within an individual tumor. PpIX production levels between various tumor lines *in vitro* have been found to be quite heterogeneous;⁹ however, most brain tumor cell lines are known to have higher PpIX production than normal brain cells,¹⁰⁻¹² indicating that there is likely always positive contrast relative to normal brain. This data agrees with ALA-induced PpIX fluorescence *in vivo* in preclinical models as well as clinical data, where significant differences in tumor tissue removal can be achieved through fluorescence-guided surgery compared to conventional white light surgery.^{2,13}

Extensive study on human glioma patients has been completed by Stummer et al.,¹³ culminating in a multicenter clinical

[†]Current address: Beth Israel Deaconess Medical Center, Harvard Medical School, Boston MA 02215

*Address all correspondence to: Summer L. Gibbs-Strauss, Beth Israel Deaconess Medical Center, Harvard Medical School, Boston, MA 02215; E-mail: sgibbs@bidmc.harvard.edu; or Brian W. Pogue, Thayer School of Engineering, Dartmouth College, Hanover NH 03755; E-mail: Brian.W.Pogue@Dartmouth.edu

cal trial where ALA-induced PpIX fluorescence-guided resection of human gliomas was compared to conventional white light resection. The contrast-enhancing portion of the tumor, as detected by magnetic resonance imaging, was completely removed in 65% of the fluorescence-guided resections, compared to 36% of the white light surgeries. This increased 6 month progression free survival to 41% in the fluorescence-guided resection group as compared to 21.1% in the white light resection group.¹³ The ability to visualize PpIX fluorescence in brain tumor tissue over normal brain tissue via surgical guidance was motivation for this work on noninvasive detection of brain tumors due to high tumor-to-normal brain tissue PpIX fluorescence signals.

Following earlier studies completed *in vitro*,⁹ PpIX fluorescence was explored for its ability to delineate tumor-bearing animals from healthy animals in a noninvasive manner. Transmission fluorescence spectroscopy was used for noninvasive detection of PpIX fluorescence, while normalizing the signal to the transmitted excitation light signal.¹⁴ Even through use of this transmission geometry, the PpIX fluorescence signal from the mouse skin was found to influence measurements, so skin photobleaching was explored as a method to increase PpIX signal contrast between tumor-bearing animals and healthy animals.¹⁵⁻¹⁷

2 Materials and Methods

2.1 Cell Culture

Two cell lines were used in the studies presented; the 9L rat gliosarcoma cell line transfected with green fluorescent protein (9L-GFP) and the human glioma cell line U251. The 9L-GFP cell line was a generous gift from Alexi Bogdanov.¹⁸ The cell lines were cultured in Dulbecco's modification of eagle's medium (Cellgro, Mediatech, Herndon, Virginia), supplemented with 10% fetal bovine serum (Atlanta Biologicals, Lawrenceville, Georgia) and 1% penicillin/streptomycin from a stock solution of 10,000 IU penicillin and 10,000 $\mu\text{g}/\text{ml}$ streptomycin (Mediatech, Herndon, Virginia), and were kept incubated at 37°C in a 95% air and 5% carbon dioxide humidified environment.

2.2 Murine Glioma Model

Both cell lines (9L-GFP and U251) were used for intracranial implantation into male athymic nude mice about 6 weeks of age. Mice were anesthetized using ketamine/xylazine in a 90:10-mg/kg ratio, and their body temperature was maintained during anesthesia via a heating pad. A small incision was made in the scalp exposing the top of the skull so that the landmarks on the brain were visible. A Dremel drill was used to make a 1-mm hole in the skull, located 2 mm in front of the bregma and 2 mm to the left of the midline, after which the needle was inserted 2 mm deep into the brain via guidance from a stereotactic frame. A total of 1×10^6 cells in 10 μl of phosphate buffered saline (PBS) were injected over 5 min using a Hamilton syringe. After the injection, the needle was slowly retracted, the skull was cleaned to ensure cells were not deposited outside the brain, and bone wax was used to cover the hole drilled in the skull. Finally, the incision in the scalp was closed with a small amount of Vetbond Tissue Adhesive (J.A. Webster, Inc., Sterling, Massachusetts). Mice

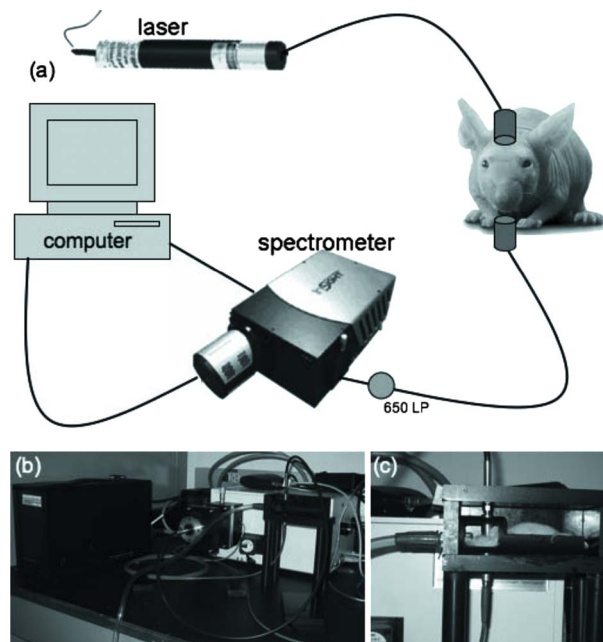


Fig. 1 (a) A schematic of the single channel spectroscopy system is shown containing a 635-nm laser, a spectrometer, a 650-nm LP filter, and a computer. In (b), a photograph of the system with the light tight box open is shown. In (c), a sample mouse is shown in the holder in position for measurement.

were examined daily following surgery to ensure proper healing of the scalp. Control mice were implanted with 10- μl PBS without cells to allow similar surgical procedures to be performed on all mice.

2.3 Single Channel Fluorescence Spectroscopy System

A schematic of the single channel spectroscopy system can be seen in Fig. 1(a). The system consisted of a 250-mW, 635-nm diode laser (Power Technology, Incorporated) for excitation collimated onto the chin of the mouse. The light transmitted through the mouse head was collected through a second collimator, and passed through a 650-nm LP filter prior to spectrally resolved detection through a spectrometer (1200-l/mm grating, SpectraPro 300, Acton Research, Acton, Massachusetts) and onto a cooled charge-coupled device (CCD) camera (Spec-10:400BR/XTE, Princeton Instruments, Acton, Massachusetts). Data from the camera were captured and transferred using commercial software (Winspec, Acton Research). The spectrometer was centered at 705 nm to collect the PpIX fluorescence emission peak, and at 615 nm to collect the transmitted intensity from the 635-nm laser. A mouse holder consisted of a bed in a light tight box with holes 180-deg apart from one another to hold the collimators, for collection of spectroscopy data [Figs. 1(b) and 1(c)].

2.4 Spectroscopy Data Collect and Processing

At each time point, the mouse was placed in the mouse holder with the collimators in contact with the head. Fluorescence emission data was collected with the spectrometer centered at 705 nm, and the exposure time adjusted to obtain signals in the linear range of the spectrometers with maximal signal-to-

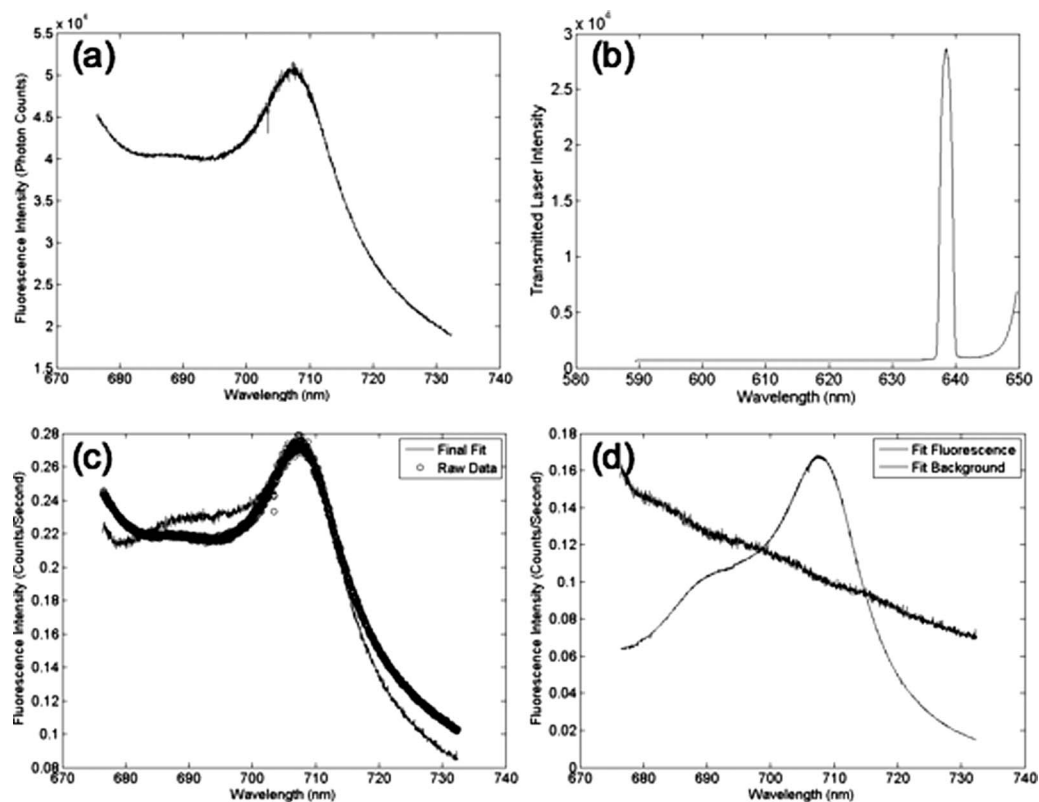


Fig. 2 In (a), the PpIX fluorescence emission data are plotted for a sample mouse. In (b), the transmittance spectrum from the 635-nm laser through the head of a sample mouse is shown. In (c), the PpIX fluorescence data are spectrally fitted to a reference PpIX spectrum from tissue-simulating phantom data. In (d), the deconvolved fluorescence and nonspecific background signals are shown.

noise level. The light was passed through the 650-nm LP filter to collect the PpIX fluorescence emission prior to detection by the spectrometer [Fig. 2(a)]. Prior to any movement of the mouse, transmittance data were also collected, where the spectrometer was centered at 615 nm to allow detection of the 635-nm laser intensity through the 650-nm LP filter, and the exposure time was again adjusted to ensure detection in the linear range of the spectrometers [Fig. 2(b)].

The raw spectral excitation and emission data were post-processed by a two-step process involving spectral fitting and then normalization. PpIX fluorescence data were collected using a liquid tissue simulating phantom composed of 1% Intralipid to simulate scattering, 1-mg/L India ink to simulate absorption, 1- $\mu\text{g}/\text{mL}$ PpIX in dimethyl sulfoxide to simulate *in vivo* PpIX concentrations, and 5% Tween 20 to decrease aggregation of PpIX, a hydrophobic molecule, in solution. The spectral shapes of PpIX obtained from these tissue-simulating phantoms were normalized to one and used for spectral fitting of *in vivo* PpIX data. The fluorescence data were spectrally fitted using a MatLab program to perform a linear least squares fit to the PpIX phantom data, so that the nonspecific background signal could be deconvolved from the PpIX fluorescence signal [Figs. 2(c) and 2(d)], as it had a distinctly different spectral shape. The area under the deconvolved PpIX fluorescence curve was then calculated and reported as a single number. Both the fluorescence emission data and the transmittance data were normalized to counts/second to account for differences in exposure time. Then the

integrated fluorescence intensity was normalized to the integrated transmitted laser intensity to account for positional differences between measurements of a single mouse, as well as variations in optical properties,¹⁴ resulting in the fluorescence-to-transmittance ratio.

2.5 Protoporphyrin IX Detection of Brain Tumors

At 10 to 14 days after tumor implantation, the mice were imaged via a large bore Philips 3T Magnetic Resonance Imaging (MRI) Achieva system, using a modified rodent body coil insert.¹⁹ A plastic insert was used in the rodent coil to raise the mouse into the isocenter of the magnetic field [Figs. 3(a) and 3(b)]. Intracranial tumors were identified using T1 turbo spin echo (TSE) images with and without Gadolinium enhancement (1- $\mu\text{l}/\text{mg}$ body weight) [Fig. 3(c)], as well as T2 TSE imaging sequences. T1 TSE and T2 TSE images were also collected prior to sacrifice for *in vivo* and *ex vivo* tumor comparison.

Prior to ALA administration, the mice were placed in the single channel spectroscopy mouse holder and their background PpIX fluorescence was measured while they were under inhaled isoflurane anesthesia. The mice were then administered 100-mg/kg ALA dissolved in PBS by intraperitoneal (IP) injection. Two hours after ALA administration, the PpIX fluorescence was again measured using the single channel spectroscopy system. The mice were then sacrificed, their brains extracted, and placed back into the spectroscopy sys-

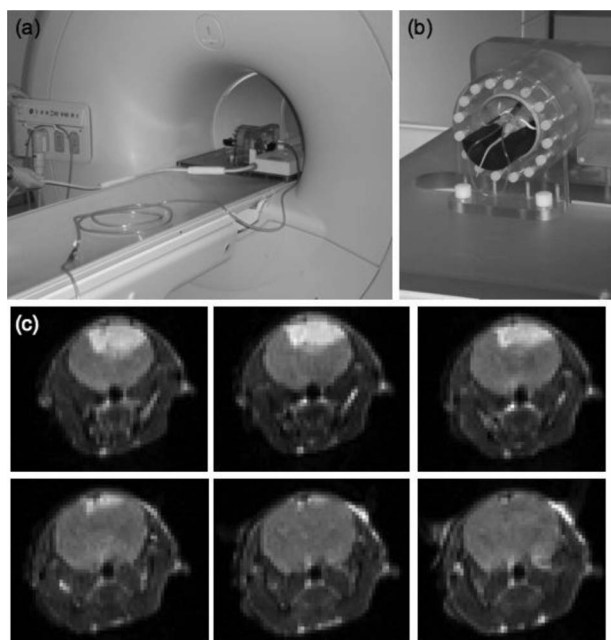


Fig. 3 In (a), the rodent coil inside the 3T MRI is shown, and in (b) an example mouse in the rodent coil with IP catheter for Gd-DTPA injection is shown. In (c), a sample set of T1 coronal turbo spin echo contrast enhanced (TSE-CE) images are shown for a 9L-GFP tumor.

tem for *ex vivo* measurement of the tumor *in situ*. Following collection of all spectroscopy measurements, the brain was sectioned in a coronal plane and imaged on a fluorescence plate scanner (Typhoon 9410, GE Healthcare Life Sciences) with the cut faces of the brain facing the imaging plane of the scanner. The tissue slices were imaged for PpIX fluorescence using a 633-nm excitation laser and a 650-nm LP emission filter, and when appropriate, then scanned for GFP fluorescence using a 488-nm laser with a 526-nm SP emission filter. Following fluorescence imaging, the brain slices were sent to pathology for routine hematoxylin and eosin (H&E) staining.

2.6 Red Light Time Course Photobleaching

Four control mice, nine 9L-GFP tumor-bearing mice, and seven U251 tumor-bearing mice were compared in this study. In each group the tumors were implanted, identified via MRI, and the PpIX fluorescence of each mouse was then measured using the single channel spectroscopy system as described previously. Following the measurement 2 h after the administration of ALA, the 635-nm laser was left running and subsequent measurements were collected after 1, 2, 4, 8, 16, 24, and 32 min to allow for photobleaching of the skin PpIX fluorescence signal.

2.7 Statistical Analysis

Differences between all groups were established through box and whisker plots and unpaired two-tailed students-t tests to establish *p*-values for comparison of all groups of interest. All box and whisker plots shown illustrate the median as the center line and the interquartile range as the enclosed box showing 75% of the data. The upper whisker represents $Q3 + 1.5(Q3 - Q1)$ and the lower whisker represents

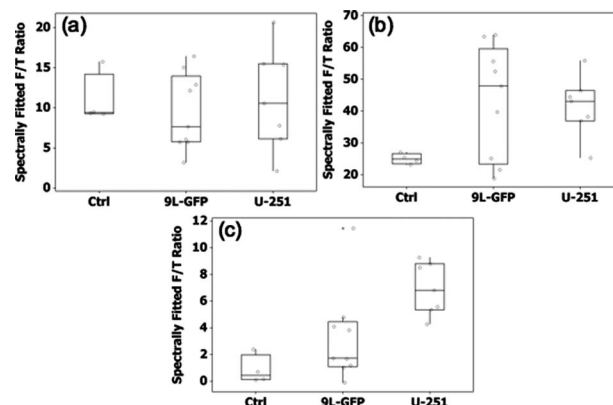


Fig. 4 The PpIX fluorescence-to-transmittance signal ratio (F/T ratio); (a) prior to ALA administration *in vivo*, (b) 2 h after ALA administration *in vivo*, and (c) 2 h after ALA administration, measured *ex vivo* on the extracted whole brain.

$Q1 - 1.5(Q3 - Q1)$, where *Q* is the quartile. Each open circle represents the fluorescence-to-transmittance ratio of one mouse.

The ability to quantify PpIX fluorescence spectroscopy as a method to detect tumors was assessed by receiver operator characteristic (ROC) analysis. The values for sensitivity and specificity were estimated based on the number of true positives, false positives, true negatives, and false negatives, where tumor status was confirmed through MRI and histology. Sensitivity was calculated as the number of true positive (TP) cases divided by the number of true positive and false negative (FN) cases [sensitivity = $TP / (TP + FN)$]. Specificity was calculated as the number of true negative cases (TN) divided by the number of true negative and false positive (FP) cases [specificity = $TN / (TN + FP)$].²⁰

ROC curves were constructed using different intensity threshold levels on the PpIX fluorescence-to-transmittance ratio collected from the control, 9L-GFP, and U251 tumor-bearing mice. As the intensity threshold was changed, the true positive fraction (TPF) and false positive fraction (FPF) were calculated, where TPF is synonymous with sensitivity and FPF is representative of 1 minus the specificity of the tumor detection modality. The area under the curve (AUC) was calculated from the ROC curves and used as a direct measure of sensitivity and specificity of the spectroscopy system for tumor detection. An AUC of 1 would indicate that the tumor detection modality had 100% sensitivity and specificity of detection, while an AUC of 0.5 would indicate there was only 50% sensitivity and specificity, equivalent to random guessing of tumor status.

3 Results

3.1 Protoporphyrin IX Fluorescence Detection of Brain Tumors

At 18 to 22 days following tumor implantation, the mice were measured in the single channel spectroscopy system prior to ALA administration, 2 h after ALA administration and *ex vivo* following brain extraction. As can be seen in Fig. 4(a), prior to the administration of ALA the mean PpIX fluorescence of the control mice, 9L-GFP, and U251 tumor-

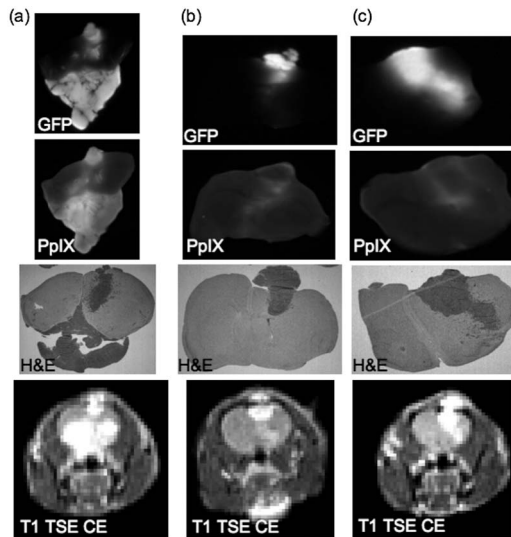


Fig. 5 Images of mouse brain tissue with 9L-GFP tumors shown with *ex vivo* GFP (first row), PpIX (second row), and H&E (third row) of the same sections of the brain. Also, in the bottom row, *in vivo* T1 turbo spin echo contrast enhanced (TSE-CE) MRI of approximately the same section. In (a), the PpIX fluorescence can be seen in the bulk tumor as compared to the H&E stained image and the GFP fluorescence image. In (b) and (c), the PpIX fluorescence was observed only at the periphery of the tumor tissue, not in the bulk tumor as can be seen by comparing the PpIX fluorescence image with the corresponding H&E stained images and GFP fluorescence images.

bearing mice were very similar. However, 2 h after the administration of ALA, there was a significant difference between the means of the control group and the 9L-GFP tumor-bearing group (p -value=0.016), as well as between the means of the control group and the U251 tumor-bearing group (p -value=0.004). The mean PpIX fluorescence of the 9L-GFP and U251 groups were similar 2 h after ALA administration; however, the variance of the 9L-GFP group was large compared to that of the U251 group [Fig. 4(b)]. Following sacrifice, *ex vivo* measurements were collected on the bulk brain tissue. As can be seen in Fig. 4(c), the mean fluorescence of the 9L-GFP group was slightly higher than that of the control group, while the mean fluorescence of the U251 group was significantly higher than either the control group (p -value<0.0001) or the 9L-GFP group (p -value=0.021).

3.2 Protoporphyrin IX Tumor Tissue Production Heterogeneity

PpIX production following ALA administration was heterogeneous between mice, as can be seen in Fig. 5, which shows three sample 9L-GFP tumor-bearing mice. For each mouse the same brain section is shown in a PpIX fluorescence image, a GFP fluorescence image, and an H&E stained image. Approximately the same section can be viewed *in vivo* via the T1 turbo spin echo (TSE) Gadolinium contrast enhanced MR image. Figure 5 illustrates that while some of the 9L-GFP mice showed PpIX production in the bulk tumor, as can be seen in Fig. 5(a), most of the 9L-GFP mice only had PpIX fluorescence on the periphery of the tumor tissue and virtually no increase in PpIX fluorescence in the bulk tumor tissue over the surrounding normal brain tissue [Figs. 5(b) and 5(c)]. The

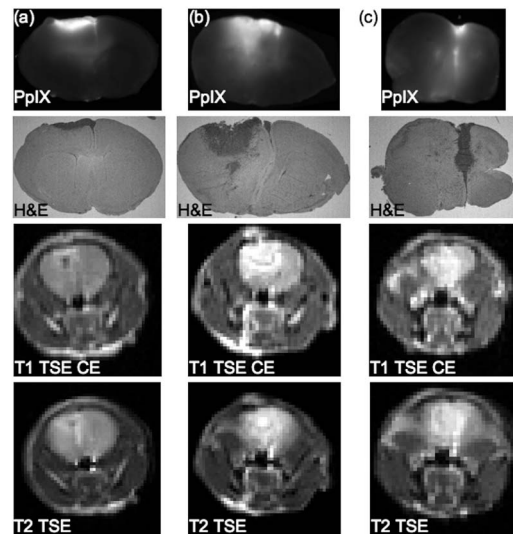


Fig. 6 Images of mouse brain tissue with U251 tumors shown with *ex vivo* PpIX fluorescence images (first row) and corresponding H&E stained images (second row) of the same sections of the brain. *In vivo* T1 turbo spin echo contrast enhanced (TSE-CE) MRI (third row) and T2 TSE MR images (fourth row) of approximately the same section shown in *ex vivo* images. In (a), (b), and (c), all mice exhibit increased PpIX fluorescence corresponding to the bulk tumor area as can be seen by comparing the PpIX fluorescence images with the corresponding H&E stained images.

pattern of tumor tissue PpIX production in the 9L-GFP gliosarcoma model was very different from that seen in the U251 glioma model. Figure 6 shows that the PpIX production in the U251 tumors was confined to the bulk tumor when compared to the H&E stained section in all three examples. It can also be seen that the T1 TSE Gadolinium-enhanced MR images and T2 TSE MR images allowed for *in vivo* visualization of approximately the same tumor tissue section shown *ex vivo*.

3.3 Red Light Time Course Photobleaching

Due to high PpIX production in skin tissue, selective photobleaching of skin PpIX fluorescence should improve noninvasive tumor tissue detection. The mean PpIX fluorescence measured 2 h after ALA administration showed a different relationship between the control group and the two tumor-bearing groups than that seen by *ex vivo* PpIX measurements. Specifically, the 2-h *in vivo* measurements showed the 9L-GFP group with slightly higher mean PpIX fluorescence than the U251 group (mean PpIX fluorescence: control=25.02, 9L-GFP=43.20, U251=41.50), as can be seen in Fig. 4(b), while the *ex vivo* measurements illustrated that the mean PpIX fluorescence of the U251 group was more than twice that of the 9L-GFP group (mean PpIX fluorescence: control=0.85, 9L-GFP=3.3, U251=6.9) as reported in Fig. 4(c). The time course photobleaching measurements were examined to determine if the red light photobleaching facilitated *in vivo* visualization of the same PpIX fluorescence contrast pattern seen in *ex vivo* measurements.

A similar relationship to that seen 2 h after the administration of ALA was seen after 1, 2, and 4 min of red light photobleaching, where the mean PpIX fluorescence of the 9L-GFP group was slightly higher than that of the U251 group.

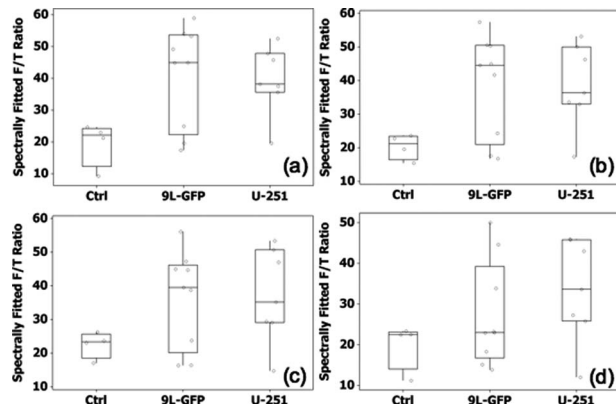


Fig. 7 The PpIX fluorescence-to-transmittance ratio (F/T ratio) of the mice in the control group and each tumor-bearing group after (a) 1 min, (b) 2 min, (c) 4 min, and (d) 8 min of red light photobleaching. The mean of the U251 group was higher than the mean of the 9L-GFP group for the first time following ALA administration in the photobleaching time course after 8 min of red light photobleaching.

The measurement obtained after 8 min of red light photobleaching showed the mean PpIX fluorescence of the U251 group was higher than in the 9L-GFP group, which was the same relationship that was seen in the *ex vivo* measurements. Box and whisker plots that showed the individual mice in each group as well as the interquartile range can be seen in Fig. 7 for the mice after 1, 2, 4, and 8 min of red light photobleaching. The measured PpIX fluorescence of the 9L-GFP group was considerably reduced following 8 min of red light photobleaching, the mean of which was lower than the U251 group (mean PpIX fluorescence: control=19.92, 9L-GFP =27.24, U251=33.38).

3.4 Receiver Operator Characteristic Analysis

Detection of tumor-bearing animals over nontumor-bearing control animals via ALA-induced PpIX fluorescence spectroscopy before and after red light photobleaching was assessed by ROC analysis. ROC curves were plotted for each tumor

type relative to the control animals 2 h after ALA administration, but prior to any photobleaching [Fig. 8(a)] and after 8 min of red light photobleaching [Fig. 8(b)]. Two hours after ALA administration, prior to any photobleaching, the U251 tumor-bearing group could be detected with higher sensitivity and specificity than the 9L-GFP tumor-bearing group, compared to the control group (U251 AUC=0.94, 9L-GFP AUC=0.72). Following the 8 min of red light photobleaching, detection sensitivity and specificity were decreased in both tumor-bearing groups over the control group; however, the decrease was more significant in the 9L-GFP tumor-bearing group than in the U251 tumor-bearing group. This decrease in detection sensitivity could be attributed to increased overlap between the PpIX fluorescence-to-transmittance ratio of the tumor-bearing group and the control group (U251 AUC=0.92, 9L-GFP AUC=0.69).

4 Discussion

Two brain tumor lines with very different tissue PpIX production patterns were studied *in vivo*. The 9L-GFP and U251 tumor lines were examined for their ability to detect brain tumor presence noninvasively via spectroscopic measurements of PpIX fluorescence. Prior to the administration of ALA, tumor-bearing mice could not be distinguished from control mice via *in vivo* PpIX spectroscopy measurements [Fig. 4(a)]. At 2 h after ALA administration, the average PpIX fluorescence in both tumor-bearing groups was significantly higher than in the control group (p -value 9L-GFP=0.016, p -value U251=0.004 relative to control). Thus, on average a tumor-bearing mouse could be detected over a normal mouse by noninvasive *in vivo* PpIX spectroscopy measurements [Fig. 4(b)]. ROC analysis revealed detection sensitivity and specificity were significantly higher for the U251 group (AUC =0.94) than for the 9L-GFP group (AUC=0.72) [Fig. 8(a)]. This difference in PpIX fluorescence between the tumor-bearing groups and the control group was confirmed through *ex vivo* PpIX spectroscopy measurements. Both tumor-bearing groups had higher mean PpIX fluorescence than the control group, as can be seen in Fig. 4(c), although the 9L-GFP group

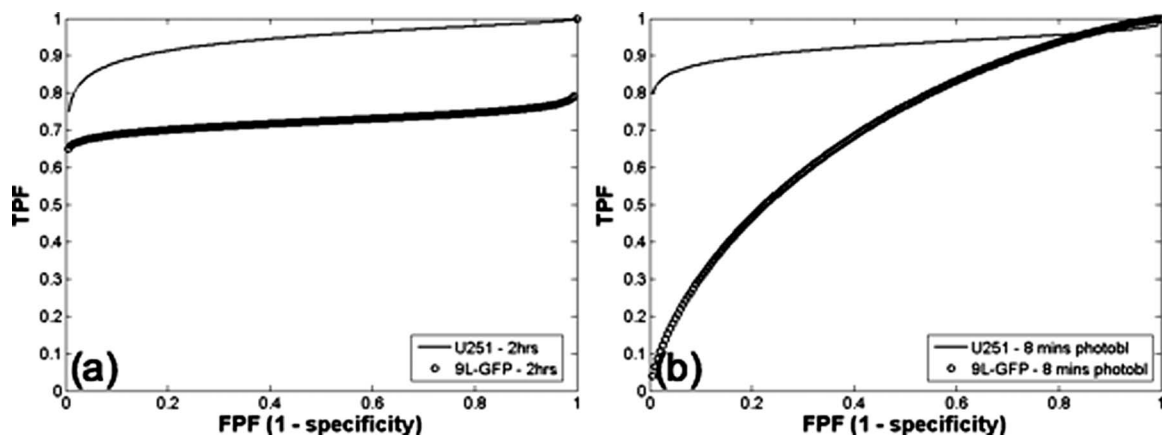


Fig. 8 Receiver operator characteristic (ROC) curve for PpIX fluorescence-to-transmittance ratio of U251 tumor-bearing group versus control nontumor-bearing group and 9L-GFP tumor-bearing group versus control group. The area under the curve (AUC) was calculated as a metric to compare tumor detection sensitivity and specificity for the two tumor types over control, nontumor-bearing animals. The ROC curve for PpIX fluorescence tumor detection (a) 2 h after ALA administration where the U251 AUC=0.94 and the 9L-GFP AUC=0.72, and (b) after 8 min of red light photobleaching where the U251 AUC=0.92 and the 9L-GFP AUC=0.69.

was only slightly higher than the control group, explaining its lower sensitivity and specificity of detection *in vivo* as compared to the U251 group [Fig. 8(a)].

The variance in PpIX fluorescence following the administration of ALA seen in the 9L-GFP tumor-bearing group via *in vivo* spectroscopy measurements was quite large in comparison to the U251 tumor-bearing group or the control group [PpIX fluorescence standard deviation (SD): control SD = 1.64, 9L-GFP SD = 17.7, U251 SD = 9.45]. A similar pattern of variance was seen in the *ex vivo* spectroscopy measurements, where the 9L-GFP group had a larger standard deviation than the U251 group, which was slightly larger than the standard deviation of the control group (PpIX fluorescence SD: control SD = 1.1, 9L-GFP SD = 3.5, U251 SD = 1.9). The varied ability of the 9L-GFP tumors to produce PpIX fluorescence could be explained when the PpIX production pattern of the tissue was examined in comparison to the GFP fluorescence and H&E stained section. Figure 5(a) showed the pattern of PpIX fluorescence expected prior to examination of the 9L-GFP tumor-bearing group *ex vivo*. The PpIX fluorescence was confined to the bulk tumor tissue, which could be seen when the PpIX fluorescence images were compared to both the GFP fluorescence images and the corresponding H&E images. However, many of the mice in the 9L-GFP group had a PpIX production pattern more like that illustrated in Figs. 5(b) and 5(c), where the PpIX fluorescence in the bulk tumor was similar to that in the surrounding normal brain, and increased production of PpIX was only visible in the periphery of the tumor. These two different production patterns would lead to high variability of PpIX fluorescence signal *in vivo*, as some tumor-bearing mice in the 9L-GFP group would appear to have high PpIX fluorescence, when the entire tumor produced PpIX [Fig. 5(a)], while other mice in the 9L-GFP group would appear to have relatively low PpIX fluorescence, when only the periphery of the tumor produced PpIX [Figs. 5(b) and 5(c)].

The PpIX fluorescence standard deviation in the U251 tumor-bearing group was considerably smaller than in the 9L-GFP group by both *in vivo* and *ex vivo* spectroscopy measurements. As can be seen in Fig. 6, the PpIX production pattern in the U251 group was significantly different from that in the 9L-GFP group. All of the mice in the U251 group showed extensive PpIX production in the bulk tumor tissue and much higher PpIX signal in the tumor tissue over the surrounding normal brain tissue. Thus, PpIX fluorescence signal detected via spectroscopy was not as variable as that of the 9L-GFP group since all the U251 mice had PpIX production which corresponded well to content of the brain tumor tissue. This decrease in PpIX production heterogeneity of the U251 tumor model compared to the 9L-GFP tumor model translated to increased sensitivity and specificity of detection over the control animals (U251 AUC = 0.94, 9L-GFP AUC = 0.72).

Skin photobleaching was examined for its ability to increase PpIX contrast between tumor-bearing mice and control mice. Due to the high PpIX production of the skin, the *in vivo* spectroscopic measurements included PpIX produced in the brain tissue as well as PpIX produced in the skin. Theoretically, photobleaching of skin PpIX fluorescence could increase the difference in PpIX signal between control mice and tumor-bearing mice, even though the overall measured signal would be decreased. In the red light photobleaching experi-

ment, the average PpIX fluorescence following the administration of ALA, but prior to any skin photobleaching, was higher in the 9L-GFP tumor-bearing group than in the U251 tumor-bearing group. However, the *ex vivo* spectroscopy measurements illustrated that the average PpIX fluorescence of the U251 group was more than twice that of the 9L-GFP group. The PpIX fluorescence measurements obtained during the time course of red light photobleaching were considered to determine if the ability to quantify the average PpIX contained in the brain tumor tissue was improved. As shown in Fig. 7(d), after 8 min of red light photobleaching, a similar relationship to that seen in the *ex vivo* data [Fig. 4(c)] was visible by *in vivo* spectroscopy measurements, where the highest mean PpIX fluorescence was seen in the U251 group, followed by the 9L-GFP group, and then the control group.

The sensitivity and specificity of detection as measured by AUC through ROC analysis were decreased by the red light photobleaching compared to 2 h after ALA administration but prior to any photobleaching. This decrease in sensitivity and specificity was due to increased overlap of the PpIX fluorescence-to-transmittance ratio of the tumor-bearing animals and the control animals (U251 AUC = 0.92, 9L-GFP AUC = 0.69) [Fig. 8(b)]. Following photobleaching, the shape of the ROC curve for the 9L-GFP tumor-bearing animals was significantly different from that prior to photobleaching (Fig. 8). The sensitivity of detection could be increased to 100% after photobleaching, although at this level of sensitivity to tumor presence, the specificity of detection was significantly decreased and caused detection of false positives. Skin photobleaching was advantageous in the detection of the 9L-GFP tumors because, due to the 9L-GFP tumor PpIX production heterogeneity, 100% sensitivity in detection of these tumors was not possible without photobleaching. In the case where tumor PpIX production was heterogeneous and tumor detection was of most importance, skin photobleaching would be advantageous due to its ability to increase sensitivity to tumor presence. In contrast, when specificity was most important, skin photobleaching would not be advantageous, as it significantly decreased the specificity of detection for the 9L-GFP tumor-bearing group.

5 Conclusions

In conclusion, noninvasive PpIX spectroscopy measurements are able to detect the presence of both the 9L-GFP tumors and U251 tumors over nontumor-bearing mice using the average PpIX fluorescence of each group as the metric. The variance in PpIX production is quite large in the 9L-GFP tumor-bearing group compared to the U251 group or the control group. This PpIX production difference can be explained through tumor tissue PpIX production patterns, where some of the 9L-GFP tumors have high PpIX fluorescence in the bulk tumor, while others have increased PpIX fluorescence only in the periphery of the tumor with little increase in PpIX fluorescence in the bulk tumor tissue. Red light skin photobleaching decreases the contrast between the tumor-bearing groups and the control group, but increases the ability to quantify the PpIX fluorescence contained within the brain tissue over the PpIX fluorescence in the skin. A noninvasive, low-cost fluorescence-based detection system has been demonstrated to be useful for detection of brain tumor models,

although sensitivity and specificity of noninvasive detection of tumors is influenced by the PpIX production pattern of the model tumor tissue. This system could potentially be extended to other laboratory tumor models following *ex vivo* studies to confirm tumor burden corresponded to PpIX fluorescence intensity, which appears to be model dependent.

Acknowledgments

The authors are grateful to Nathan Watson and Mark Israel for use of the U251 tumor cell line and for informative discussions about the glioma lines and data. This work has been funded by NCI grants RO1CA109558 and PO1CA84203, as well as the Norris Cotton Cancer Center Shared Resources.

References

1. J. C. Kennedy, S. L. Marcus, and R. H. Pottier, "Photodynamic therapy (PDT) and photodiagnosis (PD) using endogenous photosensitization induced by 5-aminolevulinic acid (ALA), mechanisms and clinical results," *J. Clin. Laser Med. Surg.* **14**(5), 289–304 (1996).
2. A. Bogaards A. Varma, S. P. Collens, A. Lin, A. Giles, V. X. Yang, J. M. Bilbao, L. D. Lilje, P. J. Muller, and B. C. Wilson, "Increased brain tumor resection using fluorescence guidance in a preclinical model," *Lasers Surg. Med.* **35**(3), 181–190 (2004).
3. W. Stummer, A. Novotny, H. Stepp, C. Goetz, K. Bize, and H. J. Reulen, "Fluorescence guided resection of glioblastoma multiforme by using 5-aminolevulinic acid-induced porphyrins, a prospective study in 52 consecutive patients," *J. Neurosurg.* **93**(6), 1003–1013 (2000).
4. W. Stummer, S. Stocker, W. Wagner, H. Stepp, F. Clemens, C. Goetz, A. Goetz, R. Kiefmann, and H. J. Reulen, "Intraoperative detection of malignant gliomas by 5-aminolevulinic acid-induced porphyrin fluorescence," *Neurosurgery* **42**(3), 518–526 (1998).
5. S. Collaud, A. Juzeniene, J. Moan, and N. Lange, "On the selectivity of 5-aminolevulinic acid-induced protoporphyrin IX formation," *Curr. Med. Chem.* **4**(3), 301–316 (2004).
6. Q. Peng, T. Warloe, K. Berg, J. Moan, M. Kongshaug, K. E. Giercksky, and J. M. Nesland, "5-Aminolevulinic acid-based photodynamic therapy. Clinical research and future challenges," *Cancer* **79**(12), 2282–2308 (1997).
7. S. A. Friesen, G. O. Hjortland, S. J. Madsen, H. Hirschberg, O. Engbraten, J. M. Nesland, and Q. Peng, "5-Aminolevulinic acid-based photodynamic detection and therapy of brain tumors (review)," *Int. J. Oncol.* **21**(3), 577–582 (2002).
8. S. B. Brown, E. A. Brown, and I. Walker, "The present and future role of photodynamic therapy in cancer treatment," *Lancet Oncol.* **5**(8), 497–508 (2004).
9. S. L. Gibbs, B. Chen, J. A. O'Hara, P. J. Hoopes, T. Hasan, and B. W. Pogue, "Protoporphyrin IX level correlates with number of mitochondria, but increase in production correlates with tumor cell size," *Photochem. Photobiol.* **82**(5), 1334–1341 (2006).
10. S. M. Wu, Q. G. Ren, M. O. Zhou, Q. Peng, and J. Y. Chen, "Protoporphyrin IX production and its photodynamic effects on glioma cells, neuroblastoma cells and normal cerebellar granule cells *in vitro* with 5-aminolevulinic acid and its hexylester," *Cancer Lett.* **200**, 123–131 (2003).
11. F. Duffner, R. Ritz, D. Freudenstein, M. Weller, K. Dietz, and J. Wessels, "Specific intensity imaging for glioblastoma and neural cell cultures with 5-aminolevulinic acid-derived protoporphyrin IX," *J. Neuro-Oncol.* **71**, 107–111 (2005).
12. S. Eleouet, N. Rousset, J. Carre, V. Vonarx, C. Vilatte, C. Louet, Y. Lajat, and T. Patrice, "Heterogeneity of delta-aminolevulinic acid-induced protoporphyrin IX fluorescence in human glioma cells and leukemic lymphocytes," *Neurol. Res.* **22**, 361–368 (2000).
13. W. Stummer, U. Pichlmeier, T. Meinel, O. D. Wiestler, F. Zanella, H. J. Reulen, and A. L.-G. S. Group, "Fluorescence-guided surgery with 5-aminolevulinic acid for resection of malignant glioma, a randomised controlled multicentre phase III trial," (see comment) *Lancet Oncol.* **7**(5), 392–401 (2006).
14. V. Ntziachristos, G. Turner, J. Dunham, S. Windsor, A. Soubret, J. Ripoli, and H. Shih, "Planar fluorescence imaging using normalized data," *J. Biomed. Opt.* **10**(6), 064007-1-8 (2005).
15. H. S. de Bruijn, A. van der Ploeg-van den Heuvel, H. J. Sterenborg, and D. J. Robinson, "Fractionated illumination after topical application of 5-aminolevulinic acid on normal skin of hairless mice, The influence of the dark interval," *J. Photochem. Photobiol., B* **85**(3), 184–190 (2006).
16. A. Johansson, T. Johansson, M. S. Thompson, N. Blendsoe, K. Svanberg, S. Svanberg, and S. Andersson-Engels, "In vivo measurement of parameters of dosimetric importance during interstitial photodynamic therapy of thick skin tumors," *J. Biomed. Opt.* **11**(3), 034028 (2006).
17. V. Nadeau, M. O'Dwyer, K. Hamdan, I. Tait, and M. Padgett, "In vivo measurement of 5-aminolevulinic acid-induced protoporphyrin IX photobleaching, a comparison of red and blue light of various intensities," *Photodermatol. Photoimmunol. Photomed.* **20**(4), 170–174 (2004).
18. A. Moore, E. Marecos, M. Simonova, R. Weissleder, and A. Bogdanov, "Novel gliosarcoma cell line expressing green fluorescent protein: a model for quantitative assessment of angiogenesis," *Microvasc. Res.* **56**, 145–153 (1998).
19. S. C. Davis, B. W. Pogue, R. Springett, C. Leussler, P. Mazurkewitz, S. B. Tuttle, S. L. Gibbs-Strauss, S. Jiang, H. Dehghani, and K. D. Paulsen, "Magnetic resonance-coupled fluorescence tomography scanner for molecular imaging of tissue," *Rev. Sci. Instrum.* **79**(6), 064302 (2008).
20. B. W. Pogue, S. C. Davis, X. Song, B. A. Brooksby, H. Dehghani, and K. D. Paulsen, "Image analysis methods for diffuse optical tomography," *J. Biomed. Opt.* **11**(3), 033001 (2006).